AD_____

Award Number: W81XWH-10-1-0713

TITLE: Magnetic Resonance Characterization of Axonal Response to Spinal Cord Injury

PRINCIPAL INVESTIGATOR: David Hackney

CONTRACTING ORGANIZATION: Beth Israel Deaconess Medical Center, Inc.
Boston, MA 02215

REPORT DATE: October 2011

TYPE OF REPORT: Annual

PREPARED FOR: U.S. Army Medical Research and Materiel Command
Fort Detrick, Maryland 21702-5012

REPORT DOCUMENTATION PAGE

Form Approved
OMB No. 0704-0188

1. REPORT DATE *(DD-MM-YYYY)*	2. REPORT TYPE	3. DATES COVERED *(From - To)*
01-10-2011	Annual	27 Sep 2010 - 26 Sep 2011

4. TITLE AND SUBTITLE
Magnetic Resonance Characterization of Axonal Response to Spinal Cord Injury

5a. CONTRACT NUMBER

5b. GRANT NUMBER
W81XWH-10-1-0713

5c. PROGRAM ELEMENT NUMBER

6. AUTHOR(S)
David Hackney

E-Mail: dbh@post.harvard.edu

5d. PROJECT NUMBER

5e. TASK NUMBER

5f. WORK UNIT NUMBER

7. PERFORMING ORGANIZATION NAME(S) AND ADDRESS(ES)
Beth Israel Deaconess Medical Center, Inc.
Boston, MA 02215

8. PERFORMING ORGANIZATION REPORT NUMBER

9. SPONSORING / MONITORING AGENCY NAME(S) AND ADDRESS(ES)
U.S. Army Medical Research and Materiel Command
Fort Detrick, Maryland 21702-5012

10. SPONSOR/MONITOR'S ACRONYM(S)

11. SPONSOR/MONITOR'S REPORT NUMBER(S)

12. DISTRIBUTION / AVAILABILITY STATEMENT
Approved for Public Release; Distribution Unlimited

13. SUPPLEMENTARY NOTES

14. ABSTRACT

During the first year we pursued studies of q-space imaging (QSI) of the spinal cord and myelin imaging. The QSI studies extended our previous work establishing our ability to define the distribution of axon fiber diameters using this noninvasive approach. This work was presented at the Annual Meeting of the International Society of Magnetic Resonance in Medicine in Montreal, May, 2011. In addition, we made great progress with an ultra-short TE (UTE) method for myelin imaging. Using this approach we were able to establish quantitative accuracy vs. MR spectroscopy and preparations with known myelin content. This method holds promise for extension to human subjects, and it could offer a unique opportunity to observe myelin without confounding by other axonal injury or edema. This work was presented at the Annual Meeting of the International Society of Magnetic Resonance in Medicine in Montreal, May, 2011, and at the Annual Meeting of the American Society of Neuroradiology in Seattle, June, 2011. A revised manuscript is currently under review at the Proceedings of the National Academy of Sciences.

15. SUBJECT TERMS
Spinal Cord Injury, Magnetic Resonance Imaging, Q-Space Imaging, Ultra Short TE Imaging, Axonal Loss, Myelin

16. SECURITY CLASSIFICATION OF:			17. LIMITATION OF ABSTRACT	18. NUMBER OF PAGES	19a. NAME OF RESPONSIBLE PERSON
a. REPORT	b. ABSTRACT	c. THIS PAGE			USAMRMC
U	U	U	UU	29	19b. TELEPHONE NUMBER *(include area code)*

Table of contents

Introduction

During the first year we pursued studies of Magnetic Resonance q-space imaging (QSI) of the spinal cord and myelin imaging. The QSI studies extended our previous work establishing our ability to define the distribution of axon fiber diameters using this noninvasive approach. This work was presented at the Annual Meeting of the International Society of Magnetic Resonance in Medicine in Montreal, May, 2011. In addition, we made great progress with an ultra-short TE (UTE) method for myelin imaging. Using this approach we were able to establish quantitative accuracy vs. MR spectroscopy and preparations with known myelin content. This method holds promise for extension to human subjects, and it could offer a unique opportunity to observe myelin without confounding by other axonal injury or edema. This work was presented at the Annual Meeting of the International Society of Magnetic Resonance in Medicine in Montreal, May, 2011, and at the Annual Meeting of the American Society of Neuroradiology in Seattle, June, 2011. A revised manuscript is currently under review at the Proceedings of the National Academy of Sciences. We began implementation of the human reduced field of view diffusion imaging and inhomogeneous magnetization transfer myelin imaging.

Body

We have made significant progress on the planned activities for the first year of the award. These are summarized below. Since this is a true partnership, the activities are integrated, and there is of necessity a substantial amount of repetition from the progress reports for each PI. The only alternative to this is to attempt to isolate the work at each institution, but reporting in this manner would make it nearly impossible to follow. There would be blanks each time work crossed institutional boundaries.

We have successfully implemented the ultra short TE (UTE) imaging approach to quantify myelin. Versions of this work were presented at Annual Meeting of the International Society of Magnetic Resonance in Medicine in Montreal, May, 2011, and at the Annual Meeting of the American Society of Neuroradiology in Seattle, June, 2011. A revised manuscript, attached, is currently under review at the Proceedings of the National Academy of Sciences. The detailed data are provided in the paper, the following is a brief summary. Conventional MR imaging of the central nervous systems studies water protons exclusively. Although other compounds, such a lipid and proteins, have abundant protons the signal of these fades far too rapidly, due to their short T2, to permit detecting them with conventional techniques. Methods have been developed for identifying water protons whose behavior is closely enough linked to myelin that they permit estimates of myelin by viewing the myelin water fraction (MWF). This approach is promising, but since diseases that injure myelin also can alter water proton behavior, the MWF methods always face a confound on this basis. We have endeavored to image myelin lipid protons directly, rather than limit ourselves to myelin water. The extremely short T2 of myelin protons required implementation of an ultra-short TE (UTE) method that would detect these signals.

Using this method we studied purified myelin preparations as well as excised rat spinal cord.

Below find a plot of the proton spectrum of a purified myelin suspension and rat spinal cord in D2O. Note that the spinal cord curve is a near perfect match for the “myelin” curve, derived from a protein-free suspension. Thus, the entire spinal cord white matter signal with this method derives from myelin lipid, and there is not a contribution from myelin protein. Although quantifying myelin protein might be useful, as a practical matter any method that relied on, or included signal from, protein would need to distinguish myelin from other proteins. Our results demonstrate that this method reports myelin lipid fraction alone, without the confound of myelin, or other, proteins.

$_1$H NMR spectra of purified bovine myelin suspended in D_2O (red) and D_2O exchanged rat thoracic SC (black).

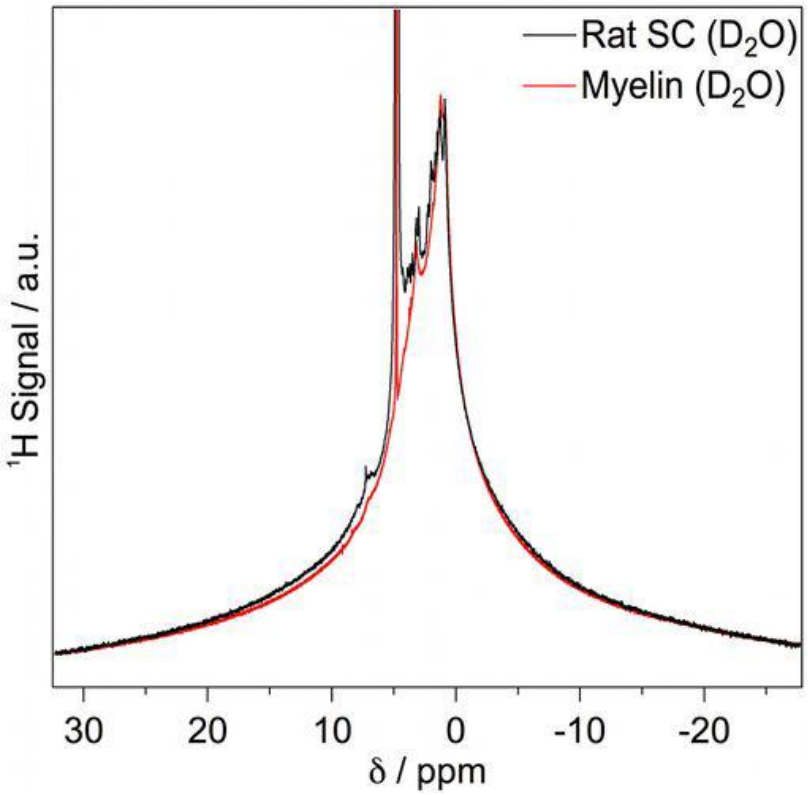

We have shown that the approach produces quantitatively reliable estimates of myelin content as assessed with graded concentrations of a D2O suspension of myelin lipid extract.

The Figure displays fitted myelin peaks for myelin suspensions of graded concentrations

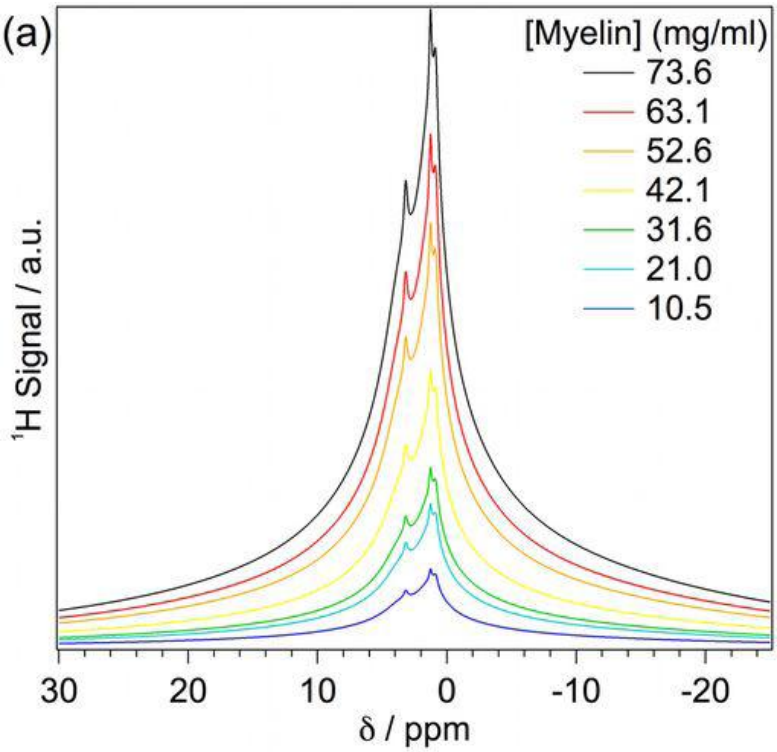

Based on these data, we determined the relationship between myelin signal intensity and known myelin concentration in suspension, finding a very high correlation (R^2=0.99)

Linear correlation plot of MR signal as a function of myelin concentration for the total (triangle), myelin (circle), and HDO (square) signal components.

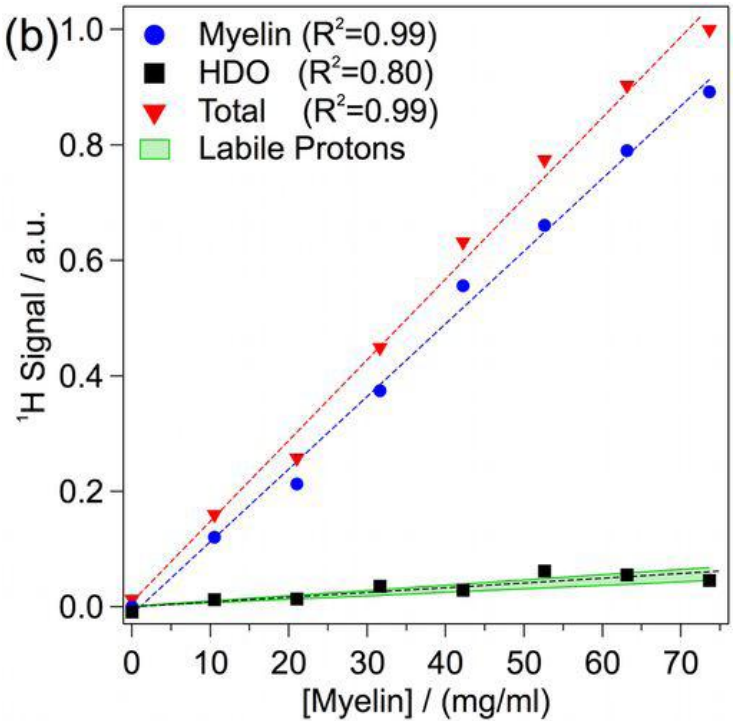

This quantitative reliability of direct myelin imaging appears to be a novel finding in this field.

This work was performed on normal cords to provide a starting point without the complications arising from spinal cord injury. However, the investigators at Drexel have been generating injured cords and these excised specimens are being imaged at Penn.

Another element of the work is q-space imaging (QSI) to measure axonal density and the axonal diameter distribution (ADD). This employs an analysis of diffusion imaging data that permits estimates of diffusion path lengths through tissue. Since spinal cord injury results in loss of axon fibers, selective loss of larger diameter fibers, and shrinkage of some surviving axons there is an overall shift to smaller diameters. To date, it has been difficult to detect this shift and hence to determine the severity of axonal damage after SCI. The challenges imposed by converting to a new imager have delayed implementation of the QSI portion of the study. Therefore, no QSI data was acquired in the first year. However, the instrument is up and running and we are now beginning to image the injured cords.

Key Research Accomplishments

- Developed high resolution UTE imaging technique for spinal cord specimens
- Developed analysis approach for UTE data
- Analyzed spinal cord specimens UTE data to produce estimates of myelin content
- Correlated imaging and spectroscopic data with known myelin suspensions and confirmed excellent quantitative accuracy
- Demonstrated that the method reports myelin lipid, but not myelin protein, content, thus is not confounded by other protein present in the spinal cord
- Prepared excised injured cords to permit UTE and QSI studies in tissue with a range of myelin and axon deficits

Reportable Outcomes

Abstracts presented

M.J. Wilhelm, H.H. Ong, S.L. Wehrli, P.-H. Tsai, D.B. Hackney, and F.W. Wehrli "Prospects for quantitative imaging of myelin with dual-echo short inversion time 3D UTE MRI"19th ISMRM, Montreal, Quebec, Canada, May 7-13, (2011).

Wilhelm, M. J.' Ong, H. H.,Wehrli, S. L.' Tsai, P.' Wright, A. C.' Hackney, D. B.'Wehrli, F. W. Prospects for Quantitative Imaging of Myelin with Ultrashort TE 3D Radial MR Imaging. 49th Annual Meeting of the American Society of Neuroradiology, Seattle, WA, June, 2011.

M.J. Wilhelm, H.H. Ong, S.L. Wehrli, P.-H. Tsai, A.C. Wright, D.B. Hackney, and F.W. Wehrli "Direct quantitative imaging of myelin with dual-echo, ultra-short TE, 3D radial MRI" 37th Pendergrass Symposium, Philadelphia, PA, June 10, (2011).

Manuscript submitted

"Direct magnetic resonance detection of myelin and prospects for quantitative imaging of myelin density". Michael J. Wilhelm, Henry H. Ong, Suzanne L. Wehrli, Ping-Huei Tsai, David B. Hackney, and Felix W. Wehrli. (revision under review at PNAS), attached

Conclusions

Although we were delayed due to technical limitations, we have successfully implemented ultra short TE imaging of the spinal cord, and shown that this is a reliable quantitative marker of myelin lipid. We are now expanding these studies, and q-space imaging to a set of excised injured spinal cord specimens we have prepared. We will then be able to study the axon diameter distribution and the myelin content in spinal cord white matter after injury

References

See "Reportable Outcomes"

Appendices

Direct magnetic resonance detection of myelin and prospects for quantitative imaging of myelin density

Michael J. Wilhelm[a], Henry H. Ong[a], Suzanne L. Wehrli[b], Ping-Huei Tsai[a,1], David B. Hackney[c], and Felix W. Wehrli[a,2]

a. Laboratory for Structural NMR Imaging, Department of Radiology, University of Pennsylvania School of Medicine, Philadelphia, PA, 19104; b. NMR Core Facility, Joseph Stokes Jr Research Institute, The Children's Hospital of Philadelphia, Philadelphia, PA, 19104; c. Department of Radiology, Beth Israel Deaconess Medical Center, Harvard Medical School, Boston, MA, 02115

Abstract

Magnetic resonance imaging (MRI) has previously demonstrated its potential for indirectly mapping myelin density either by relaxometric detection of myelin water or magnetization transfer. Here, we investigated whether myelin can be detected and possibly quantified directly. We identified the spectrum of myelin in the spinal cord *in situ* as well as in myelin lipids extracted via a sucrose gradient method, and investigated its spectral properties. High-resolution solution ^{13}C and ^{31}P nuclear magnetic resonance (NMR) spectroscopy showed the extract composition to be in agreement with myelin's known chemical make-up. The 400 MHz ^{1}H spectrum of the myelin extract, at room temperature, consists of a narrow water resonance superimposed on a broad non-Lorentzian envelope shifted approximately 3.5 ppm upfield, suggestive of long-chain methylene protons. Superimposed on this signal were narrow components resulting from functional groups having significant degrees of internal motion. The spectrum could be modeled as a superposition of multiple Lorentzians with the largest component having a lifetime (T_2^*) < 20μs. Overall, there was a high degree of similarity in the spectral properties of extracted myelin with those found in neural white matter tissue. Using 3D radially ramp-sampled proton MRI, with a combination of inversion nulling and echo subtraction, the feasibility of direct myelin imaging *in situ* is demonstrated. Lastly, the integrated signal from myelin suspensions is shown, both spectroscopically and by imaging, to scale with concentration, suggesting the potential for quantitative determination of myelin density.

Author Contributions: M.J.W., H.H.O., and F.W.W. designed research; M.J.W., H.H.O., and S.L.W. performed research; M.J.W., H.H.O., S.L.W., P.-H.T., and F.W.W analyzed data; D.B.H., acted as a secondary editor; and M.J.W., H.H.O., and F.W.W. wrote the paper.

Key words: Myelin in situ, MRI, Myelin NMR spectrum

[1]Present address: Graduate Institute of Biomedical Electronics and Bioinformatics, National Taiwan University, Taipei 10617, Taiwan, ROC

[2]Corresponding author. University of Pennsylvania Medical Center, 1 Founders, MRI Education Center, 3400 Spruce Street, Philadelphia, PA 19104, USA. Fax: +1 215 662 7263. E-mail address: wehrli@mail.med.upenn.edu (F.W. Wehrli).

\body

Introduction

Myelin is a critical feature of nervous system white matter. It is a lipid-protein bilayer that extends from the outer membrane of glial cells (i.e. oligodendrocytes in the central nervous system (CNS)), and discretely winds around individual axonal fibers leading to an increase in conduction velocity (1). By speeding conduction and reducing axonal energy requirements, myelin makes large and complex organisms possible. Myelin also contributes to the mechanical and functional structure of the axon. In addition, some oligodendrocytic cells and precursors can support action potentials themselves (2). Deficiencies of myelin lay at the core of numerous neurodegenerative disorders such as multiple sclerosis and schizophrenia (1). These deficiencies may result from developmental or acquired abnormalities in oligodendrocyte function, which also leads to axonal degeneration. Assessment of myelin may reveal CNS abnormalities far beyond those associated with classical demyelinating diseases. Magnetic resonance imaging (MRI) of myelin has the potential to characterize not only loss of this important component of the CNS, but also to reveal axonal and supporting glial integrity and function.

A diverse assortment of experimental techniques has been applied towards the goal of observing and quantifying myelin. The common methods rely on optical microscopy of histologically stained tissue samples (3). X-ray diffraction (4) and non-linear optical techniques (5, 6) also provide insight into myelin ultrastructure. Unfortunately, all these techniques are destructive and thus applicable only to animal studies.

More recently, myelin-specific chemical contrast markers that selectively bind to myelin have emerged. Such agents are currently under development for both MRI (7) and positron-emission tomography (8). While these techniques are potentially promising, concerns over toxicity may pose significant hurdles to their clinical implementation.

So far, MRI has had the greatest impact toward non-destructive myelin assessment in both laboratory animals and humans. Further, MRI has the added benefit that signal contrast originates from endogenous protons, and hence is not reliant upon injectable chemical probes nor limited by contrast-related temporal delays. To date, two distinct MR techniques have demonstrated histologically correlated sensitivity to myelin: magnetization transfer (MT) and T_2 relaxometry. In MT, cross-relaxation between myelin protons and tissue water is exploited (9). The signal attenuation resulting from off-resonance saturation (magnetization transfer ratio) has been found to scale with myelin concentration (10). T_2 relaxometry yields T_2 spectra, typically by inversion of the Carr-Purcell echo decay using an inverse Laplace transformation (11). Spectral components with T_2 values ranging from 10 to 50 ms have been assigned to motionally restricted myelin water (12, 13) and have demonstrated strong correlation with myelin specific histologic staining (12, 14).

While MT and T_2 relaxometry have shown promise, they both rely on indirect detection of myelin through the interaction of water with myelin. This complex interaction is affected by non-myelin loss related changes, which can lead to ambiguities in data interpretation. For example, MT is sensitive not only to myelin content, but also to edema (9) and axon density (15). While T_2 relaxometry may be more closely related to myelin content (16), it is still sensitive to inflammation (17). Therefore, even though both techniques may distinguish normal from abnormal WM, they cannot specifically detect losses in myelin in conditions in which edema and other abnormalities are possible.

Direct detection of myelin with MR would remove some complications in the analysis from the intermediate effects of the interaction of water and myelin, and therefore may provide contrast specific to myelin concentration. However, direct detection is complicated by extreme motional restriction of the lipid chains in the myelin bilayer, thereby causing the protons to exhibit quasi-solid-state behavior, resulting in broad lines and, consequently, short life-time of the MR signal.

The transverse relaxation properties of myelin suggest the need for ultra-short echo-time (UTE) MRI methods, which entail collection of the free-induction decay (FID) immediately after excitation. Typical implementations include either 3D radial sampling with non-selective RF pulses (18) or 2D radial sampling with slice-selective half RF pulses and ramp sampling (19) as previously applied for the characterization of cortical bone matrix and bone water (20, 21) .

UTE MRI has also been used to image the short T_2^* signal from human brain *in vivo* (22). Unlike applications to study bone, these implementations included long T_2^* suppression methods to attenuate the tissue water signal. Tissue water, due to its rotational mobility and high concentration, has an intense long-T_2^* signal that overwhelms signal from short-T_2^* components (**Fig. S1a**). While the images indicated the short-T_2^* signal to be predominantly located in white matter (WM), no evidence was provided to link this signal to myelin.

In this work we examine the origin and nature of the short T_2^* signal of CNS tissue in freshly excised rat spinal cord (SC) in comparison with purified myelin lipid extract with multi-nuclear NMR. We further explore the potential for direct detection and quantification of myelin by UTE MRI and discuss the possibilities and technical hurdles associated with translating MRI-based quantification of myelin to the clinic.

Results

High resolution ^{1}H NMR spectra of intact spinal cord tissue and bovine myelin extract

Fig. 1 shows a comparison of the ^{1}H NMR spectra collected for a section of excised rat thoracic SC and a deuterium oxide (D_2O) suspension of myelin lipid extract. The SC was first immersed in D_2O for 24 hrs to exchange tissue water with D_2O, and hence attenuate the bulk proton signal (**Fig. S1b**). The protein-free myelin lipid sample was chemically extracted from an intact isolated myelin sample, obtained via a sucrose gradient method (see Supporting Information), and quantitatively validated with proton-decoupled ^{13}C and ^{31}P NMR spectroscopy

(**Table 1**, **S2a**, and **S2b**). Both ^{1}H spectra in **Fig. 1** show a broad non-Lorentzian envelope (*ca.* 2 kHz FWHM, 15.88 kHz full width at one tenth maximum) with a superimposed narrow water resonance originating from residual HDO. Further, with the exception of the superimposed fine structure apparent in the SC spectrum (potentially originating from proteins or metabolites not present in the myelin extract), the major features of the SC and purified myelin spectra are identical.

UTE MRI of intact spinal cord

Fig. 2 shows a set of images of freshly excised rat SC, obtained with a 3D radial, ramp-sampled, dual-echo inversion recovery UTE (de-IR-UTE) pulse sequence (**Fig. S3**). Long T_2^* tissue water signal was attenuated via adiabatic inversion and echo subtraction. Images were collected at both short (**Fig. 2a**) and long (**Fig. 2b**) TE. The magnitude difference image (**Fig. 2c**) highlights the short T_2^* signal, which predominantly results from myelin protons. We note that the difference image has nearly background intensity in grey matter (GM) regions, in agreement with the very low myelin density of GM.

MR signal dependence on myelin concentration

In order to separate the myelin and water peaks in the ^{1}H spectra of the myelin-D_2O suspensions, the spectra were modeled as a weighted sum of Lorentzians: seven for myelin and one for HDO (see Methods for details). **Fig. 3** shows the results of the multi-Lorentzian fitting analysis of the proton NMR spectrum of purified myelin suspended in D_2O. The fitting results were virtually identical for all myelin concentrations. Even though the signal envelope is very broad, there is evidence of signals from protons in moieties undergoing sufficient internal motion to give rise to relatively narrow signals (see **Fig. 3a**).

Relative signal fraction, along with associated T_2^* of the seven Lorentzian components were combined into a myelin T_2^* histogram (**Fig. 3b**), which suggests 56% of the total signal to have an effective lifetime < 20 s, or 84% < 100 μs, with narrower components (i.e. T_2^* > 500 s) accounting for only 1.25% of total signal area. **Fig. 4a** shows a series of fitted myelin signals as a function of decreasing myelin concentration. NMR signal area for the total and separate spectral components (i.e. HDO and myelin) are plotted in **Fig. 4b** indicating linear scaling with myelin concentration (R^2=0.99). We attribute the positive correlation of the water peak area with myelin concentration as resulting from labile protons from myelin constituents exchanging with D_2O to form HDO. The calculated average percentage of labile protons, for each of the ten myelin lipid components, is listed in **Table 1**. The average signal contribution from the 0.1% impurity of the D_2O solvent, calculated as the y-intercept from the line of best fit (**Fig. 4b**), was subtracted from all the HDO points yielding an estimate of the labile myelin proton signal contribution. The predicted range of signal contributions from labile protons (5.05±0.79 %) agrees well with the experimental HDO peak areas (5.38±1.57%). Given the excess D_2O used in the suspensions, it is reasonable to assume that all the labile myelin protons have exchanged with deuterium.

The inset of **Fig. 5** shows the magnitude difference 2D projection de-IR-UTE image for a series of myelin suspensions of increasing concentration. Region of interest (ROI) average intensities from each of the myelin samples in the image are plotted in **Fig. 5** and, analogous to the spectral data, are shown to be linearly correlated with myelin concentration (R^2 = 0.98).

Discussion

In this work we explored the feasibility of direct imaging and quantification of myelin by magnetic resonance as an alternative to the various indirect detection techniques currently being practiced, such as MT or T_2 relaxometry. Direct detection of myelin would remove any

ambiguities in analysis and provide a contrast specific to myelin concentration. To explore the feasibility of direct myelin imaging, we first investigated the origins of the short T_2^* signal in intact WM tissue and myelin extracts. We then presented preliminary UTE with long-T_2^* suppression images of myelin in WM.

The purity of our myelin extract was validated by 9.4T high-resolution proton-decoupled ^{31}P (**Fig. S2a**) and ^{13}C (**Fig. S2b**) NMR, showing good agreement with previously determined molar ratios (23) (**Table 1**). The slight variations are reasonable given the differences in the anatomical origin of the sample (brain vs. SC) (24), inherent variability of the measurement (25), as well as the developmentally immature nature of our sample (24). Our ^{13}C spectra also agreed well with Husted et al's reported proton-decoupled magic-angle spinning (MAS) ^{13}C NMR spectra of isolated human myelin (26). In that study a synthetic ^{13}C spectrum of myelin was generated as a weighted sum of individual lipid spectra, based upon the known ratios of the individual lipid components. The synthetic spectrum was found to be in good agreement with the observed MAS spectrum, which in turn closely matches our solution spectrum (**Fig. S2b,** except for the absence of signals assigned to protein resonances in the MAS spectrum). Furthermore, our ^1H NMR spectra show several narrow resonances expected for some of the motionally less restricted sub-groups of myelin lipids (see **Fig. 3a**).

Any conclusions from extracted or synthetically produced myelin beg the question whether the resulting material retains the biophysical properties of native myelin. It is known that in aqueous suspensions myelin lipids spontaneously self-assemble into bilayer structures (i.e. vesicles). In this enthalpy-driven process (27) the myelin lipid suspension regains a structural order reminiscent of physiological myelin minus the protein component.

Our wideline proton spectra, obtained at 400 MHz in neural tissue after deuterium exchange of tissue water, are in good qualitative agreement with relaxometric data recently reported by Horch et al. (28). The spectrum of the isolated, reconstituted myelin exhibited a very broad line with relatively narrow components centered approximately 3.5 ppm upfield from

water, consistent with methylene protons of fatty acid chains, the main constituent of myelin. Importantly, this spectrum bears a high degree of similarity with that of neural tissue, which supports the notion that, upon aqueous suspension of the extract, a bilayer structure analogous to that for native myelin is reconstituted. Furthermore, as the myelin extract is composed solely of lipids, these results suggest that protein protons provide a negligible contribution to the short-T_2^* signal in the neural tissue spectrum.

We found that the spectrum can be modeled as a sum of Lorentzians ranging in line width from 18 to 0.01 kHz (corresponding to mean lifetimes ranging from 17μs to 3ms) and a narrow resonance assignable to HDO. The myelin resonance is consistent with the super-Lorentzian lineshape of a dipolar-broadened liquid crystalline lipid system (29, 30) as suggested by several lineshape properties (31) including a small 2nd moment ($M_2 = 1.06\times10^8$ s^{-2}), a large 4th moment (M_4) to M_2 ratio ($M_4/(M_2)^2 = 6.57$), and a full width at 1/10 maximum ($\Delta\nu_{1/10}$) to FWHM ($\Delta\nu_{1/2}$) ratio greater than three ($\Delta\nu_{1/10} : \Delta\nu_{1/2} = 7$). While the super-Lorentzian lineshape theoretically cannot be described with a basis set of exponential functions, the errors resulting from using such a set may be small for the case of myelin (28).

The present multi-Lorentzian peak approach is analogous to the multi-exponential fitting of the time-domain signal decay as previously reported (28, 32). Horch et al analyzed both Carr-Purcell echo trains and FID signals of myelinated mammalian and amphibian nerves as well as synthetic myelin at 4.7 T, to yield histograms of relaxation times (28). Similar to our spectroscopic findings, the authors detected significant components with T_2^* values of 20 and 70 s, which they postulated to arise from protein and methylene protons on the myelin sheath, respectively. Our results, however, suggest that the 20 s T_2^* component arises from myelin lipids as the myelin extract showed no evidence of proteins.

In suspensions of bovine myelin suspended in D_2O, we found the integrated areas of the resulting spectra to scale linearly with myelin concentration (**Fig. 4**). A similar correlation was

observed with 2D projection de-IR-UTE images of myelin suspensions of various concentrations (**Fig. 5**), thus suggesting that quantitative myelin imaging may be feasible. Direct 3D de-IR-UTE imaging of a rat spinal cord *in situ* at 400 MHz highlights the potential of such an approach as demonstrated with images showing signal from the WM regions only. Previously, Waldman et al (22) had obtained images of the human brain using a slice-selective UTE with soft-tissue suppression, essentially showing intense signal from WM regions of the brain, which they attributed to short-T_2^* components. While it is conceivable that the longer T_2^* components of myelin were detected, the bulk of the myelin protons certainly eluded detection. As already pointed out above, we observed that 50% of the protons in myelin may have an effective T_2^* of less than 20μs. Given that Waldman et al used slice-selective half-pulses of 400-600μs duration, the magnetization from these components could not be nutated since the pulse duration is almost two orders of magnitude longer than the protons' lifetime (33).

Major hurdles would have to be overcome for translation of the method to the clinic. First, given that the bulk of the proton signal may reside in a component of myelin with an effective T_2^* of less than 20 μs, coherence losses during the RF pulse would be significant except in the case of very short durations on the order of 10-20μs (33). While the latter is feasible on clinical equipment (34), concerns about tissue heating will inevitably limit the admissible RF amplitudes. Myelin quantification, however, would not necessarily require detection of all components. Water suppression achieved, for example, via frequency-selective saturation, would not nutate the large majority of the myelin protons as long as the pulse duration is substantially longer than the lifetime of these protons (33). However, the proton signal of myelin could be attenuated via cross-relaxation (35), a possible effect that requires some scrutiny. Lastly, quantification would require a reference sample, ideally with relaxation and density properties matching myelin.

Conclusions

We have characterized the spectral properties of the myelin proton signal *in situ*, as well as in reconstituted suspensions of myelin lipid extract. Our results show that the short T_2^* component of WM originates primarily from myelin lipid protons and further that direct quantitative imaging of these protons may be feasible. Difficulties to be overcome include tissue water suppression and translation from a laboratory imaging system to clinical MRI scanners.

Materials and Methods

All MR spectroscopy and imaging experiments were performed on a 9.4 T vertical-bore spectrometer / microimaging system (Bruker DMX 400) with Micro2.5 gradients (100 G/cm maximum strength) and BAFPA40 amplifiers (Karlsruhe, Germany).

Neural tissue preparation

SC samples were harvested from healthy adult Sprague-Dawley rats (Charles River Laboratories International, Wilmington, MA) and bovine spinal columns (Bierig Brothers Veal and Lamb Products, Vineland, NJ). The rats were euthanized by carbon dioxide asphyxiation in accordance with an Institutional Animal Care and Use Committee (IACUC) approved protocol. After euthanasia, rat spinal columns were removed and the SC was dissected out.

NMR Spectroscopy

High-resolution proton-decoupled ^{13}C NMR (SW = 24kHz, NS = 36768, TD = 65536, TR = 1.36 s, $\alpha = 30^o$) and proton-decoupled ^{31}P (SW=3.23kHz, NS=8536, TD=8192, TR=1.27 s, $\alpha=30^o$) spectra were collected for samples of purified bovine myelin extract, dissolved in a (5:4:2) ternary mixture of deuterated chloroform (99.8% D, Acros Organics, Geel, Belgium), methanol (99.8% D, Acros Organics, Geel, Belgium), and 0.2M EDTA/water (99.9% D, Sigma-Aldrich Corp., St. Louis, MO).

All ^{1}H NMR spectra were collected with the following parameters: SW=100kHz, NS=256, TD=262144, TR=1.3107s, α=90^{o}. Freshly excised SC sections (<2 hr postmortem interval) were immersed in a perfluorinated oil (Fomblin-Y, Sigma-Aldrich Corp., St. Louis, MO) prior to experiments.

Spectral fitting to Lorentzian peak shapes were done in Igor Pro (WaveMetrics, Lake Oswego, OR). Each Lorentzian had three free parameters: frequency, intensity and FWHM. The total number of Lorentzians used in the fit was increased until the change in R^2 of the fit was less than 1×10^{-5}. The initial center frequency for additional Lorentzian functions was set equal to that of the global maximum peak in the resulting residual spectrum.

UTE MR Imaging

3D de-IR-UTE imaging (**Fig. S3**): SW=200kHz, TE=10/1200 s, TI=500 ms, TR=1s, FOV=15mm, matrix size = 128x128x128, number of views (NV) = 5,342. The sequence was based upon that used by Anumula et al (36). TI was determined empirically as the duration yielding optimal GM suppression (as GM is expected to have negligible myelin concentration). A refocusing gradient was applied immediately after the first readout gradient, following which a second gradient echo was collected at TE=1200 μs. A 3D image of the short T_2^* components was obtained as the magnitude difference of the two echo images (i.e. TE_1-TE_2).

A 2D projection de-IR-UTE sequence was used to image the series of myelin/D_2O suspensions to avoid signal losses resulting from settling of myelin during scanning. The Mn doped water phantom served to identify the locations of the samples in the image. All experimental parameters were identical to those used in the 3D de-IR-UTE experiments.

All image reconstruction was done in Matlab (Mathworks, Natick, MA) using a fast gridding algorithm (37) and incorporating k-space trajectory correction (38). All images were smoothed via bilinear interpolation with Image J (National Institutes of Health).

Acknowledgements

The authors acknowledge Joseph J. Sarver and Louis J. Soslowsky for providing a source of fresh rat CNS tissue. MJW acknowledges Mary A. Selak for patient guidance and assistance perfecting the sucrose gradient based isolation of myelin. This work was supported by NIH Grant T32 EB00814 and DOD Award W81XWH-10-1-0714.

References

1. Knaap MS van der, Valk J (2005) *Magnetic Resonance of Myelination and Myelin Disorders* eds Heilmann U, Mennecke-Bühler D (Springer, Berlin; New York). 3rd Ed.

2. Káradóttir R, Hamilton NB, Bakiri Y, Attwell D (2008) Spiking and nonspiking classes of oligodendrocyte precursor glia in CNS white matter. *Nat. Neurosci.* 11:450-456.

3. Wu Y, Alexander AL, Fleming JO, Duncan ID, Field AS (2006) Myelin water fraction in human cervical spinal cord in vivo. *J. Comput. Assist. Tomogr.* 30:304-306.

4. Avila RL et al. (2005) Structure and stability of internodal myelin in mouse models of hereditary neuropathy. *J. Neuropathol. Exp. Neurol.* 64:976-990.

5. Wang H, Fu Y, Zickmund P, Shi R, Cheng J-X (2005) Coherent anti-stokes Raman scattering imaging of axonal myelin in live spinal tissues. *Biophys. J.* 89:581-591.

6. Fu Y, Brandon Huff T, Wang H-W, Wang H, Cheng J-X (2008) Ex vivo and in vivo imaging of myelin fibers in mouse brain by coherent anti-Stokes Raman scattering microscopy. *Opt. Express* 16:19396-19409.

7. Frullano L, Wang C, Miller RH, Wang Y (2011) A myelin-specific contrast agent for magnetic resonance imaging of myelination. *J. Am. Chem. Soc.* 133:1611-1613.

8. Stankoff B et al. (2006) Imaging of CNS myelin by positron-emission tomography. *Proc. Natl. Acad. Sci. USA* 103:9304-9309.

9. Dousset V et al. (1992) Experimental allergic encephalomyelitis and multiple sclerosis: Lesion characterization with magnetization transfer imaging. *Radiology* 182:483-491.

10. Mottershead JP et al. (2003) High field MRI correlates of myelin content and axonal density in multiple sclerosis: A post-mortem study of the spinal cord. *J. Neurol.* 250:1293-1301.

11. Whittall K, Mackay A (1989) Quantitative interpretation of NMR relaxation data. *Mag. Res. Med.* 84:134-152.

12. Mackay A et al. (1994) In vivo visualization of myelin water in brain by magnetic resonance. *Mag. Res. Med.* 31:673-677.

13. Gulani V, Webb a G, Duncan ID, Lauterbur PC (2001) Apparent diffusion tensor measurements in myelin-deficient rat spinal cords. *Mag. Res. Med.* 45:191-195.

14. Laule C et al. (2008) Myelin water imaging of multiple sclerosis at 7T: Correlations with histopathology. *Neuroimage* 40:1575-15780.

15. Schmierer K, Scaravilli F, Altmann DR, Barker GJ, Miller DH (2004) Magnetization transfer ratio and myelin in postmortem multiple sclerosis brain. *Ann. Neurol.* 56:407-15.

16. Stanisz GJ, Kecojevic A, Bronskill MJ, Henkelman RM (1999) Characterizing white matter with magnetization transfer and T2. *Mag. Res. Med.* 42:1128-1136.

17. Laule C et al. (2004) Water content and myelin water fraction in multiple sclerosis: A T2 relaxation study. *J. Neurol.* 251:284-293.

18. Wu Y et al. (1998) Evaluation of bone mineral density using three-dimensional solid state phosphorus-31 NMR projection imaging. *Calcif. Tissue Int.* 62:512-518.

19. Robson MD, Gatehouse PD, Bydder M, Bydder GM (2003) Magnetic resonance: An introduction to ultrashort TE (UTE) imaging. *J. Comput. Assist. Tomogr.* 27:825-846.

20. Techawiboonwong A, Song HK, Wehrli FW (2008) In vivo MRI of submillisecond T2 species with two-dimensional and three-dimensional radial sequences and applications to the measurement of cortical bone water. *NMR Biomed.* 21:59–70.

21. Wu Y et al. (1999) Multinuclear solid-state three-dimensional MRI of bone and synthetic calcium phosphates. *Proc. Natl. Acad. Sci. USA* 96:1574-1578.

22. Waldman A et al. (2003) MRI of the brain with ultra-short echo-time pulse sequences. *Neuroradiology* 45:887-892.

23. Norton WT, Autilio LA (1966) The lipid composition of purified bovine brain myelin. *J. Neurochem.* 13:213-222.

24. Norton WT (1974) Isolation of myelin from nerve tissue. *Methods Enzymol.* 31:435–444.

25. Norton W (1965) The chemical composition of bovine CNS myelin. *Ann. NY Acad. Sci.* 122:77-85.

26. Husted C, Montez B, Le C, Moscarello MA, Oldfield E (1993) Carbon-13 “magic-angle” sample-spinning nuclear magnetic resonance studies of human myelin, and model membrane systems. *Mag. Res. Med.* 29:168-178.

27. Wimley WC, White SH (1993) Membrane partitioning: Distinguishing bilayer effects from the hydrophobic effect. *Biochemistry* 32:6307-6312.

28. Horch RA, Gore JC, Does MD (2011) Origins of the ultrashort-T2 1H NMR signals in myelinated nerve: A direct measure of myelin content? *Mag. Res. Med.* 66:24-31.

29. Bloom M, Holmes K, Mountford C, Williams P (1986) Complete proton magnetic resonance in whole cells. *J. Magn. Reson.* 69:73-91.

30. Wennerstrom H (1973) Proton nuclear magnetic resonance lineshapes in lamellar liquid crystals. *Chem. Phys. Lett.* 18:41-44.

31. MacKay AL (1981) A proton NMR moment study of the gel and liquid-crystalline phases of dipalmitoyl phosphatidylcholine. *Biophys. J.* 35:301-313.

32. Ramani A (2003) Another approach to protons with constricted mobility in white matter: Pilot studies using wideline and high-resolution NMR spectroscopy. *Magn. Reson. Imaging* 21:1039-1043.

33. Sussman MS, Pauly JM, Wright GA (1998) Design of practical T2-selective RF excitation (TELEX) pulses. *Mag. Res. Med.* 40:890–899.

34. Wu Y et al. (2010) Bone matrix imaged in vivo by water- and fat-suppressed proton projection MRI (WASPI) of animal and human subjects. *J. Magn. Reson. Imaging* 31:954-963.

35. Wolff SD, Balaban RS (1989) Magnetization transfer contrast (MTC) and tissue water proton relaxation in vivo. *Mag. Res. Med.* 10:135-144.

36. Anumula S et al. (2006) Measurement of phosphorus content in normal and osteomalacic rabbit bone by solid-state 3D radial imaging. *Mag. Res. Med.* 56:946-952.

37. Greengard L, Lee JY (2004) Accelerating the nonuniform fast fourier transform. *SIAM Rev.* 46:443–454.

38. Saligheh Rad H et al. (2011) Quantifying cortical bone water in vivo by three-dimensional ultra-short echo-time MRI. *NMR Biomed.* 24:855-864.

Figure Legends

Fig. 1: ^{1}H NMR spectra of purified bovine myelin suspended in D_2O (red) and D_2O exchanged rat thoracic SC (black).

Fig. 2: 3D de-IR-UTE images from rat thoracic SC averaged over five central slices. Images obtained for a) TE=10 s, b) TE=1,200 s, and c) magnitude difference (maximum intensity range decreased by a factor of two to highlight myelin signal). d) Intensity profiles across the three images (delineated as red, green and yellow lines in panels a, b and c, respectively) to show relative WM, GM and background intensity. The most intense signal, present in the short and long echo profiles, originates from residual surface water. The dashed blue line represents the average noise level. WM and GM are indicated in panel a, and arrows highlight residual surface water in panel b. The dark boundary observed at the GM/WM and WM/surface water interfaces in both echo images stems from a partial voluming of adjacent regions with different T_1 resulting in destructive interference.

Fig. 3: ^{1}H NMR spectra and analysis of purified bovine myelin extract suspended in D_2O: a) NMR spectrum and multi-Lorentzian fitting showing the resulting myelin and HDO fits, as well as the seven individual Lorentzian components of myelin (shaded). Narrow resonances, denoted with Greek letters, can be tentatively assigned as: terminal methyl ($-CH_3$) groups from long-chain fatty acid residues at 0.87 ppm (α), methylene ($-CH_2$) protons at 1.27 ppm (β), methylene alpha to carbonyls ($-C(O)-C(H_2)-$) at 1.94 ppm (γ), and olefinic ($-C(H)=C(H)-$) protons at 5.30 ppm (δ) as well as trimethyl ammonium protons ($-N^{+}(CH_3)_3$) from PC, PCpl, and Sph at 3.18 ppm (ε) and secondary amide protons ($-C(O)-N(H)-$) at 7.16 and 8.46 ppm (ζ and η). b) T_2^* histogram of myelin components derived from the multi-Lorentzian fitting. Inset shows magnified view of the longer T_2^* components.

Fig. 4: a) Fitted myelin peaks for myelin suspension of various concentrations. b) Linear correlation plot of MR signal as a function of myelin concentration for the total (triangle), myelin (circle), and HDO (square) signal components. All two tailed p-values < 0.01. Also shown is the calculated signal fraction of labile myelin protons (green shaded).

Fig. 5: UTE imaging and analysis of purified bovine myelin extract suspended in D_2O. (inset) 2D projection de-IR-UTE images of six 5mm NMR tubes filled with myelin / D_2O suspensions of varying concentrations (mg/ml). Mn indicates the tube containing manganese-doped water. Plot of the normalized de-IR-UTE mean ROI intensities vs. normalized myelin concentration (p=0.0002). Arrows indicate areas of signal from paper towel used to stabilize the tubes.

Table Legends

Table 1: Lipids of myelin with abbreviations used in the text. Comparison of average bovine myelin lipid molar ratios reported by Norton et al (23) and quantitative multi-nuclear magnetic resonance methods. Also shown are average percentage of labile protons available from each lipid component.

Myelin Lipid	ID	Molar Percentage		% Labile $^{1}H \pm \sigma$[‡]
		Norton*	NMR[†]	
Cholesterol	CHOL	44.8	43.1	0.94 ± 0.04
Galactocerebroside	GC	17.5	19.6	2.20 ± 0.39
Galactosulfatide	GS	2.5	NA[§]	0.28 ± 0.05[¶]
Phosphatidylethanolamine	PE	3.4	3.9	0.24 ± 0.05
PE Plasmalogen	PEpl	11.3	11.8	0.70 ± 0.13
Phosphatidylcholine	PC	8.0	7.8	0.00 ± 0.00
PC Plasmalogen	PCpl	0.3	2.0	0.00 ± 0.00
Sphingomyelin	Sph	5.2	5.9	0.37 ± 0.08
Phosphatidylinositol	PI	0.7	2.0	0.19 ± 0.03
Phosphatidylserine	PS	0.2	3.9	0.11 ± 0.01
Total				5.05 ± 0.79

* From Norton et al (23).
† Present study, ^{13}C and ^{31}P NMR.
‡ Variability (σ, standard deviation) due to lipid chain length [$CH_3(CH_2)_n$; n=10-25].
§ Not measured due to a lack of an unambiguous resonance.
¶ Assuming a GS molar percentage of 2.5%.

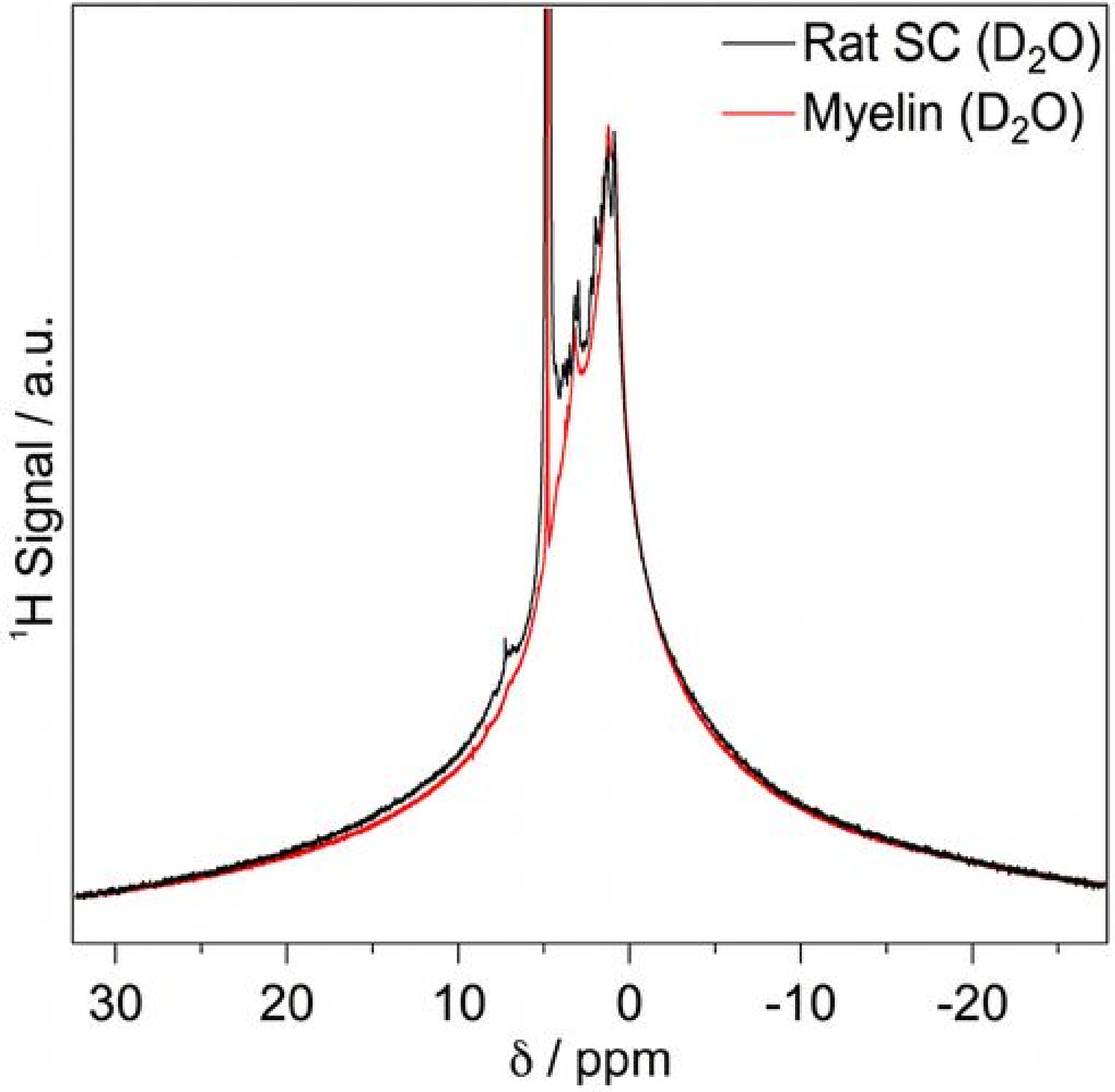
Rat SC (D_2O)
Myelin (D_2O)
^{1}H Signal / a.u.
30
20
10
0
-10
-20
δ / ppm

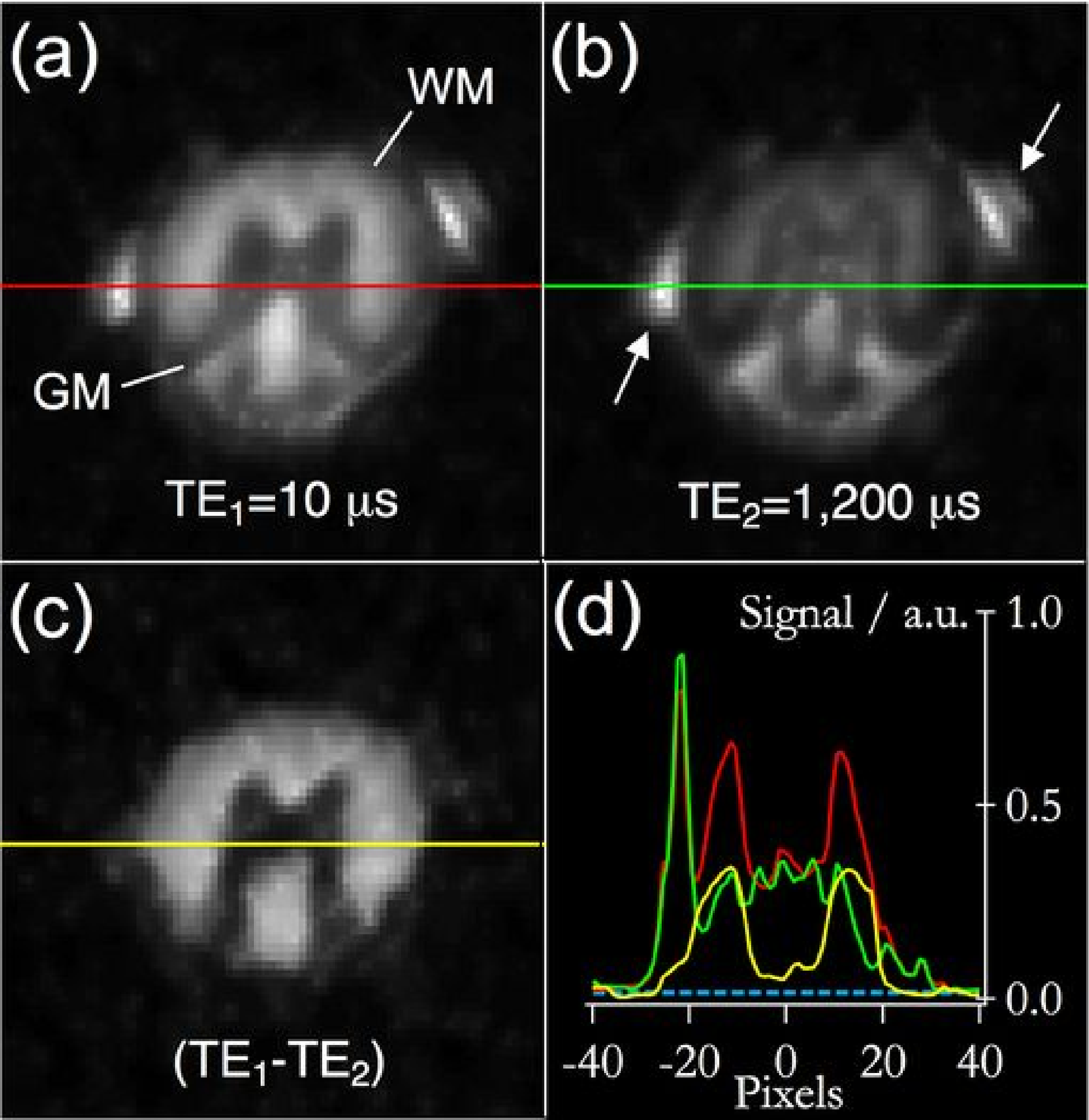
(a)
WM
GM
TE1=10 μs
(b)
TE2=1,200 μs
(c)
(TE1-TE2)
(d)
Signal / a.u.
1.0
0.5
0.0
-40
-20
0
20
40
Pixels

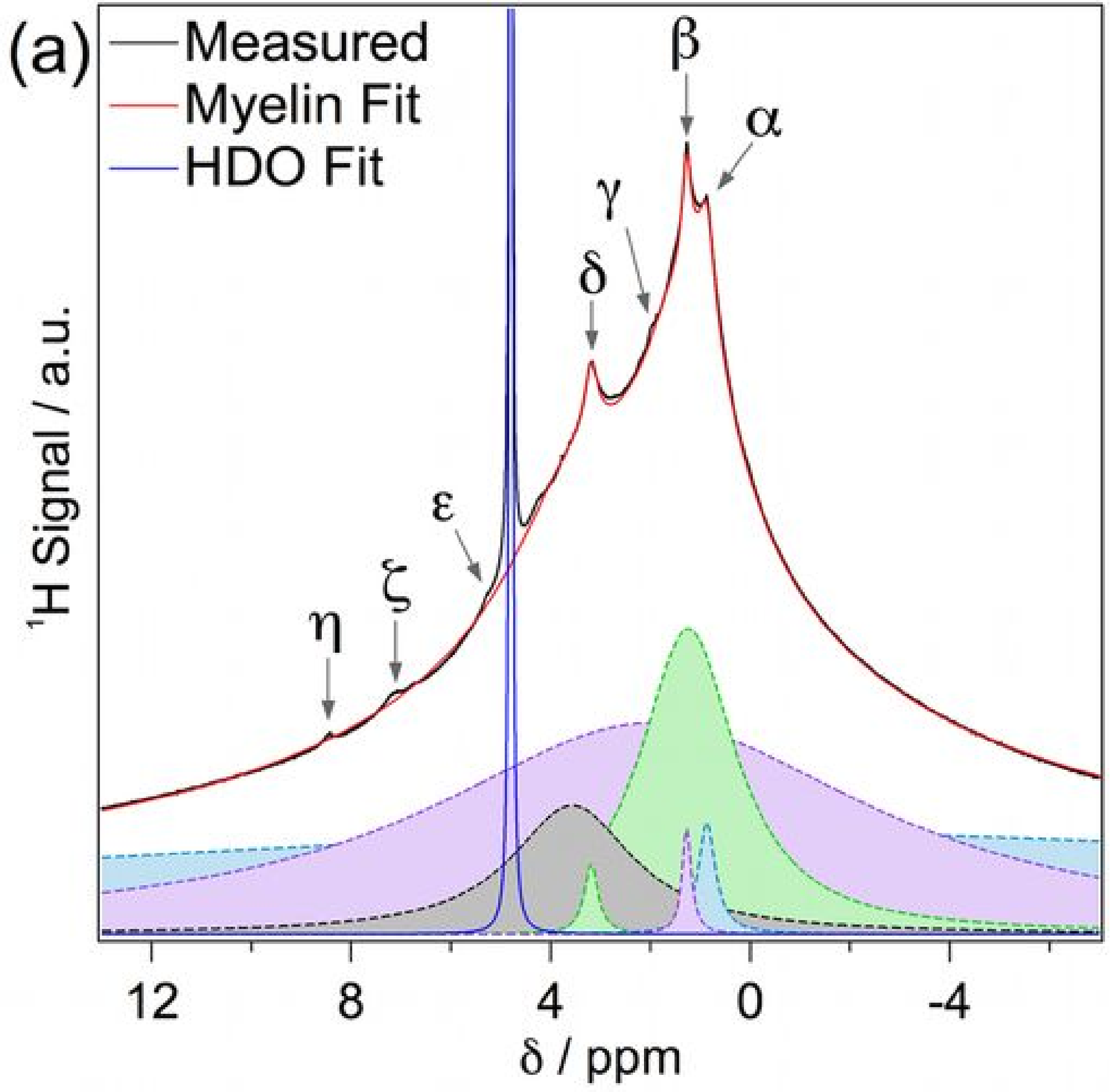
(a)
Measured
Myelin Fit
HDO Fit
β
α
γ
δ
ε
ζ
η
^{1}H Signal / a.u.
12
8
4
0
-4
δ / ppm

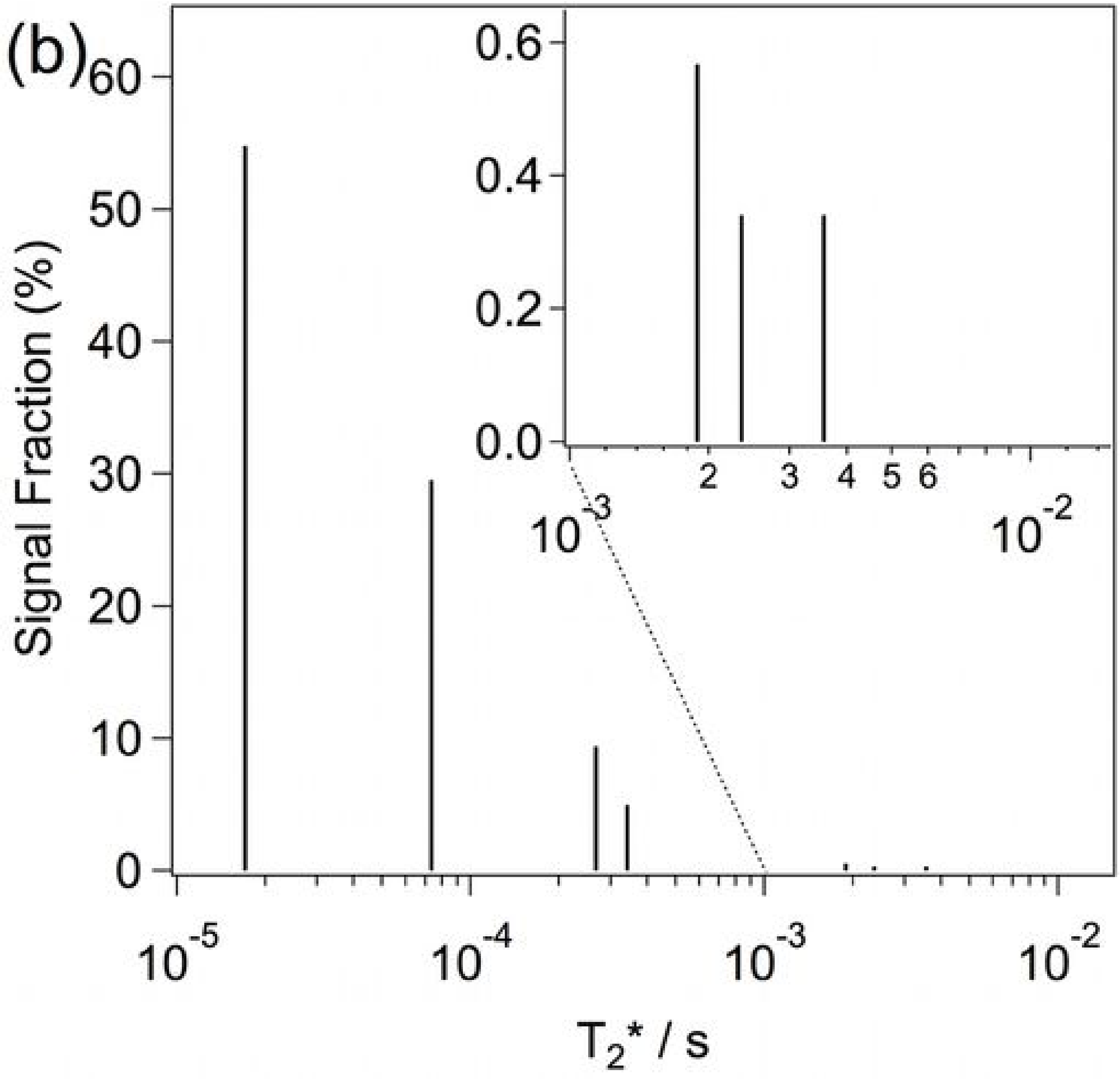
(b)
Signal Fraction (%)
0
10
20
30
40
50
60
10^{-5}
10^{-4}
10^{-3}
10^{-2}
T_2^* / s
0.0
0.2
0.4
0.6
2
3
4
5
6
10^{-3}
10^{-2}

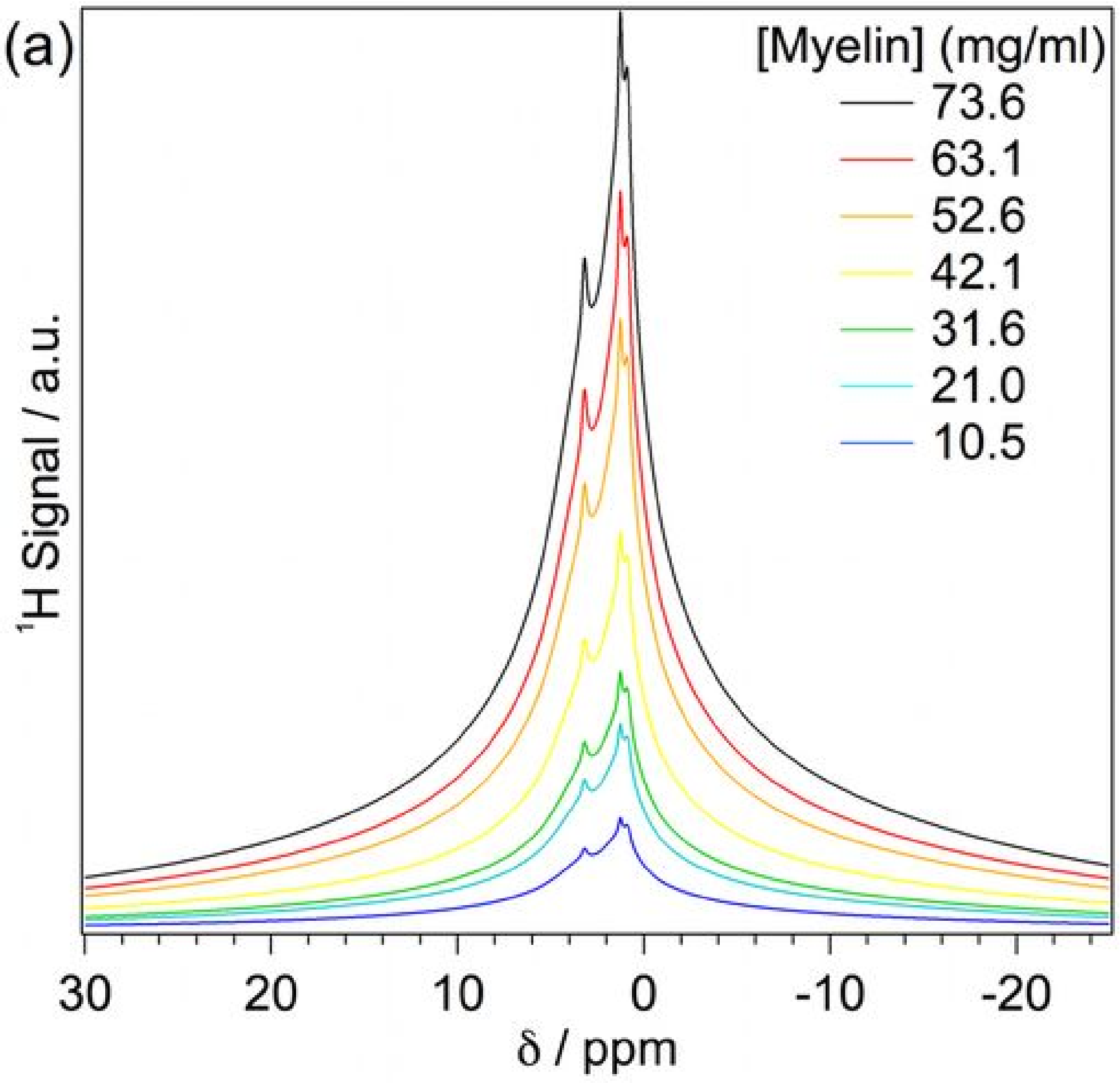
(a)
[Myelin] (mg/ml)
73.6
63.1
52.6
42.1
31.6
21.0
10.5
^{1}H Signal / a.u.
30
20
10
0
-10
-20
δ / ppm

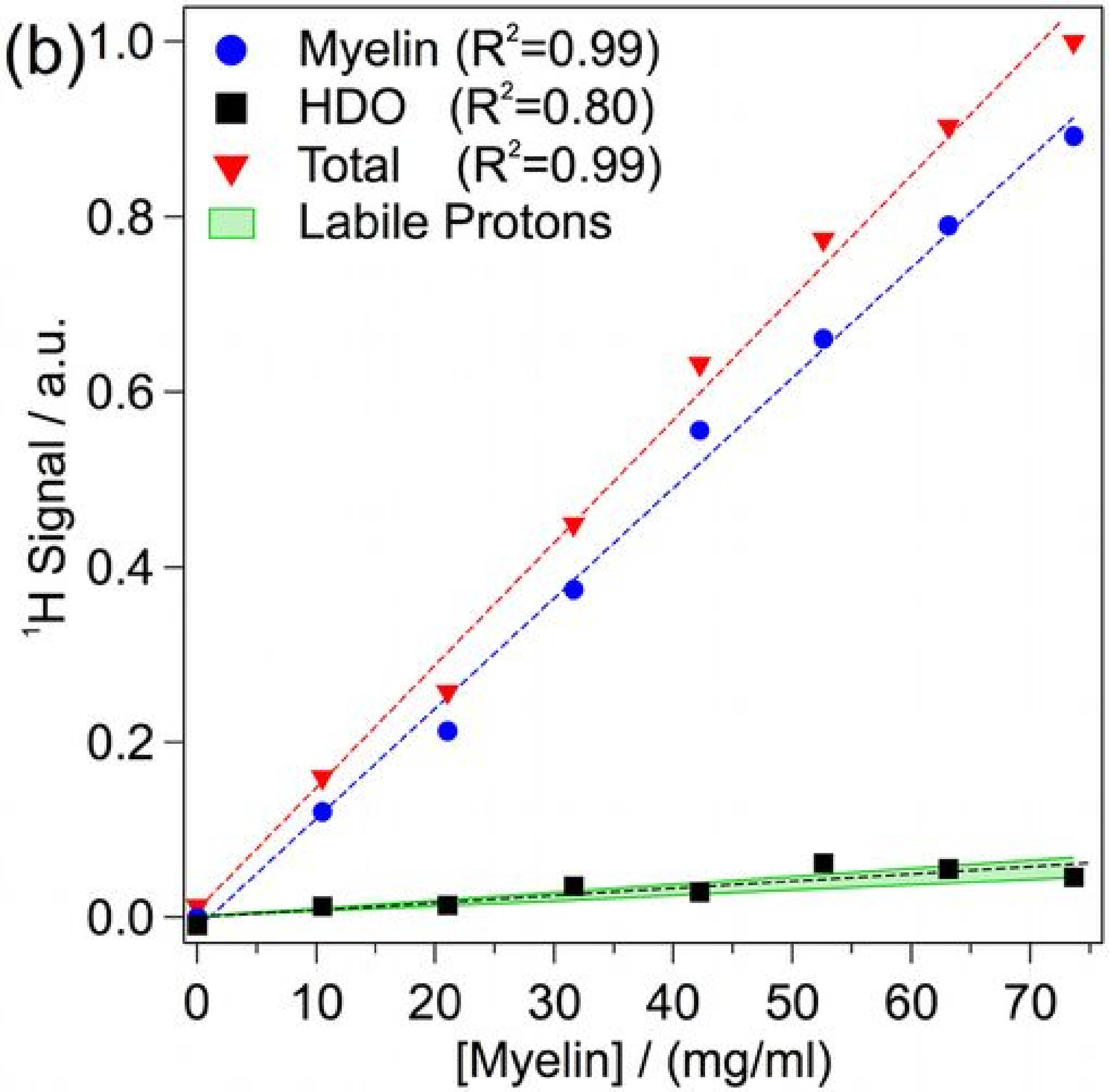
(b)
Myelin (R^2=0.99)
HDO (R^2=0.80)
Total (R^2=0.99)
Labile Protons
^{1}H Signal / a.u.
1.0
0.8
0.6
0.4
0.2
0.0
0
10
20
30
40
50
60
70
[Myelin] / (mg/ml)

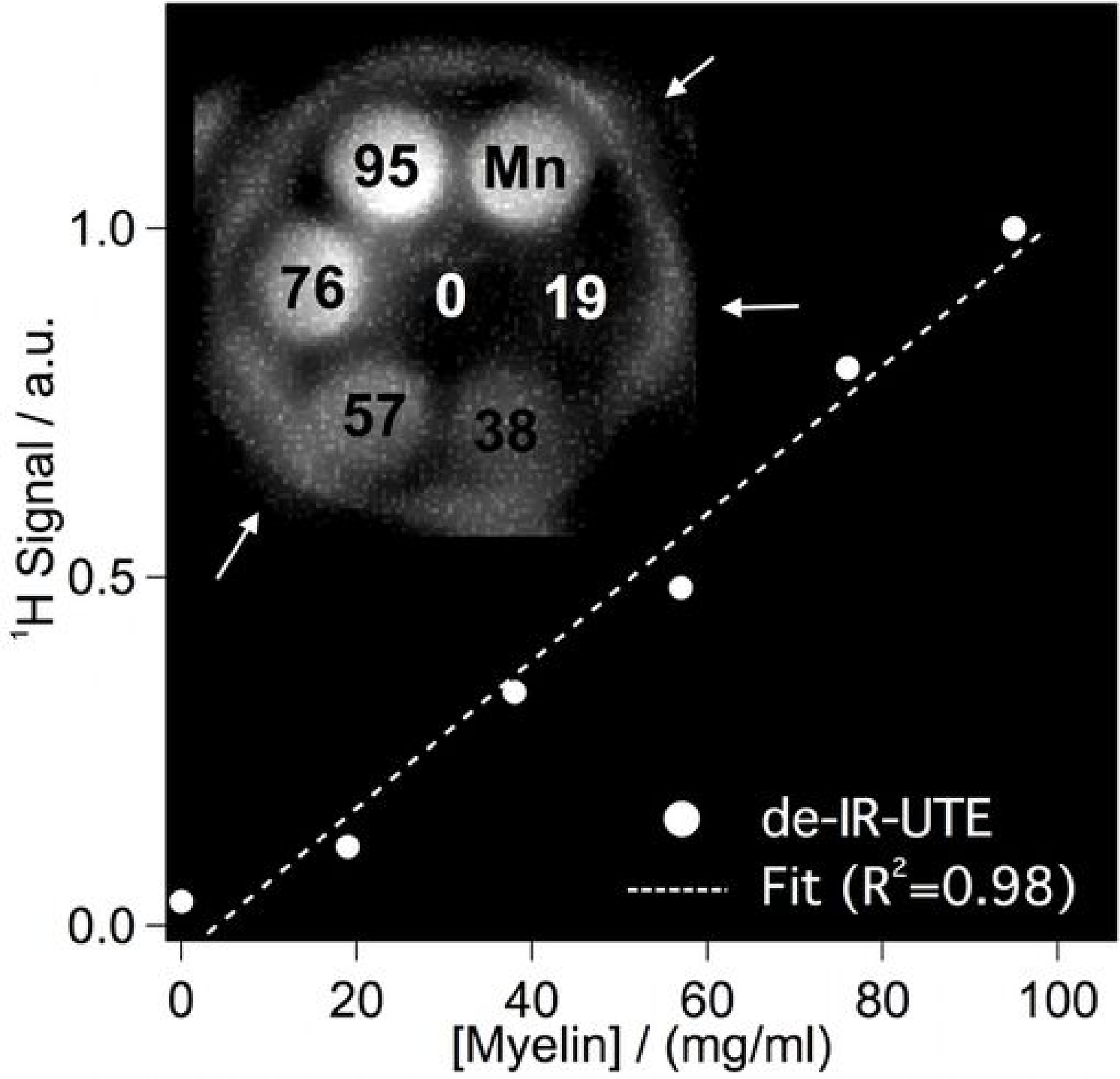
95
Mn
76
0
19
57
38
1.0
0.5
0.0
^{1}H Signal / a.u.
0
20
40
60
80
100
[Myelin] / (mg/ml)
de-IR-UTE
Fit (R^2=0.98)